A SEARCH FOR INTERSTELLAR BUBBLES SURROUNDING MASSIVE STARS IN PERSEUS OB1

C. E. CAPPA[1]

Instituto Argentino de Radioastronomía, CC 5, 1894 Villa Elisa, Argentina; and Facultad de Ciencias Astronómicas y Geofísicas, Universidad Nacional de La Plata, Paseo del Bosque s/n, 1900 La Plata, Argentina; ccappa@fcaglp.fcaglp.unlp.edu.ar

AND

UWE HERBSTMEIER

Max-Planck-Institut für Astronomie, Königstuhl 17, D-69117 Heidelberg, Germany; and Radioastronomisches Institut der Universität Bonn, Auf dem Hügel 71, D-53121 Bonn, Germany

ABSTRACT

We have examined the interstellar medium in the vicinity of massive stars belonging to the Per OB1 association based on neutral hydrogen 21 cm observations obtained with the 100 m radio telescope at Effelsberg (HPBW = 8'4) and complementary data from the Leiden-Dwingeloo H I Survey (HPBW = 36'). The higher angular resolution H I observations allowed us to discover probable wind-blown bubbles related to four massive stars in the association, namely, HD 14442 [O5n(f)p], HD 14947 [O5If+], HD 13022 [O9.5II-III((n))], and HD 13338 [O9.5V], while the detection of a wind-blown bubble associated with HD 16691 [O5If+] is less conclusive. A clear H I shell coincident in position with two B1III stars (HD 15233 and Hilt 311) was also detected. Some of these features also have infrared and/or molecular counterparts. The energetics of the structures related to each massive star is analyzed. The new H I interstellar bubbles appear to be similar to the ones found surrounding Wolf-Rayet stars and other Of stars. The large-scale maps obtained using the lower angular resolution H I data show that most of the early-type stars belonging to Per OB1 are placed in a region of low H I emission. The association could have blown a H I shell of about 350 × 550 pc in size. This large H I shell has an infrared counterpart.

Key words: ISM: bubbles — ISM: individual (Perseus OB1) — stars: early-type — stars: individual

1. INTRODUCTION

H I 21 cm line observations have shown neutral hydrogen bubbles created by a hypersonic stellar wind interacting with the surrounding interstellar medium (ISM). These interstellar wind-blown bubbles (WBBs) appear associated with a large number of Wolf-Rayet (WR) stars (e.g., Marston 1996; Arnal et al. 1999; Cappa et al. 1999, and references therein). In most cases, their large dimensions together with their low expansion velocities suggest dynamical ages of a few million years, several times longer than the duration of the WR phase of a massive star ($\approx 5 \times 10^5$ yr, Maeder & Meynet 1994), implying that the massive O-type star progenitor of the current WR star must also be responsible for the formation of the bubbles.

Consequently, O and Of stars seem to be promising candidates for showing the signature of the interaction of the stellar wind with the surrounding medium. At optical wavelengths, Lozinskaya (1982) found ring nebulae associated with a few Of stars. Several neutral hydrogen bubbles were also detected surrounding Of stars (e.g., Kutchar & Bania 1993; Cappa & Benaglia 1998; Benaglia & Cappa 1999). However, up to present, the number of well-studied associations of Of stars and H I voids and shells is too small for a comprehensive understanding of such interactions.

The analysis of the H I WBBs provides valuable information concerning the energetics and dynamics of the ISM. The comparison of these results with theoretical predictions from evolutionary models of interstellar bubbles allows us

to improve the modeling of the interaction between massive stars and the surrounding ISM.

The energy supplied to the ISM by massive stars in OB associations and open clusters also leads to the formation of shells and supershells through ionizing stellar radiation, stellar winds, and supernova explosions (e.g., Bruhweiler et al. 1980; McCray & Kafatos 1987; Mac Low & McCray 1988; Oey 1996). In particular, neutral hydrogen shells and supershells appear to be related to a certain number of galactic OB associations and open clusters (e.g., Per OB2, Sancisi 1974; Cep OB3, Simonson & van Someren Greve 1976; Upper-Centaurus Lupus and Upper-Scorpius, de Geus 1988; Ori OB1b, Chromey, Elmegreen, & Elmegreen 1989; Lac OB1, Cappa de Nicolau & Olano 1990; Ara OB1, Rizzo & Bajaja 1994; Car OB2, Rizzo 1994; and OCl 352, Normandeau, Taylor, & Dewdney 1996).

In this paper we analyze the H I gas distribution in the environs of Per OB1 with the aim of investigating the action of the strong stellar winds of O and Of stars on their surroundings.

Per OB1 is an OB association spread within an area of 8° × 6° approximately centered at $(l, b) = (134°5, -3°5)$. Humphreys (1978) derived a mean distance modulus of 11.83 (2.3 kpc) for the association from the individual stellar distances of the O-, B-, and A-type stars, in agreement with previous results from Ruprecht (1966). Garmany & Stencel (1992) obtained a distance modulus of 11.8 based on the best fit to a color-magnitude diagram for the B main-sequence stars. Distances to the open clusters *h* and *χ* Persei [NGC 869 at $(l, b) = (134°5, -3°5)$ and NGC 884 at $(l, b) = (135°1, -3°6)$], which are generally considered to be related to Per OB1, range from 2.1 to 5.5 kpc (Becker & Fenckart 1971; Janes & Adler 1982). However, Garmany & Stencel

---

cast some doubts on the fact that the clusters are related to the association. Based on these results, an optical distance of 2.3 kpc will be adopted for Per OB1.

Heiles (1979) in his search for galactic shells and super-shells, found an H I shell that correlates in position with Per OB1. This 5° diameter structure is detected in the velocity range -31 to -23 km s^{-1} (all velocities in this paper are referred to LSR). The presence of gas expanding away from Per OB1 is reinforced by studies of interstellar absorption lines in direction to several stars in the association (Münch 1957; Phillips & Gondhalekar 1981; McLachlan & Nandy 1985).

Koo, Heiles, & Reach (1992) identified in this region the *worm* candidates GW 131.3-2.2 and GW 132.6-9, in the velocity ranges -59.6 to -16.9 and -31.3 to -22.9 km s^{-1}, respectively. These *worms* were also detected in infrared and radio continuum emission at 100 and 60 μm and at 408 MHz. Heiles (1984) interpreted these structures as the walls surrounding superbubbles which have broken through the thin gaseous disk.

The stellar data of the O and Of stars that are members of Per OB1 (Garmany & Stencel 1992) are summarized in Table 1. Column (1) lists the name of the star; column (2), the galactic coordinates (l, b); column (3), its spectral classification; column (4), the stellar distance; columns (5) and (6), the stellar wind parameters; and column (7), the LSR stellar radial velocity. The stellar distances were estimated from photometric data (Nicolet 1978), and absolute magnitudes and intrinsic colors by Vacca, Garmany, & Schull (1996) and Schmidt-Kaler (1982), respectively. A typical uncertainty of 25% has been taken into account for the distances. Within errors, the individual distances agree with the optical distance to Per OB1. Values in parenthesis in

columns (5) and (6) indicate that $\dot{M}$ was derived through the fitting formula by Lamers & Leitherer (1993) as a function of the luminosity and the effective temperature of the star, and V_w corresponds to mean values obtained as a function of spectral type and luminosity class (Prinja, Barlow, & Howarth 1990). The uncertainties in $\dot{M}$ and V_w are $\simeq 0.2$ dex and 400 km s^{-1}, respectively.

Our study is based on H I 21 cm line emission data obtained with the 100 m single-dish antenna of the Max-Planck-Institut für Radioastronomie (MPIfR) at Effelsberg, Germany, with an angular resolution of 8'4, on low angular resolution observations taken from the H I survey by Hartman & Burton (1997), and on complementary infrared, radio continuum, and molecular data.

2. DATA SETS

We have performed λ21 cm H I line observations over the region of the Per OB1 association where most of its O and Of stars are projected in 1992 January and 1993 December with the Effelsberg 100 m single-dish radio telescope of the MPIfR, Bonn, Germany. A region of 27.3 deg^2 was surveyed following two different grids. Two areas of 1 deg^2 each surrounding HD 14947 and HD 16691 were sampled with a grid spacing of 5'; while a grid spacing of 10' was used for the rest of the region.

The dual-channel FET amplifier and the 1024 autocorrelation spectrometer, which was split in two halves with 512 channels each, were used to receive both independent circular polarizations. The frequency switching technique was applied with signal and reference bands 3.2 MHz apart. Table 2 lists the main parameters of the observations. The brightness temperature scale was derived from observations of the calibration point position S7 ($l = 132°$, $b = -1°$;

TABLE 1

O AND OF STARS IN PERSEUS OB1: STELLAR DATA

Name (1)	l, b (2)	Sp. Class. (3)	d (kpc) (4)	$\dot{M}$ (10^{-6} $M_\odot$ yr^{-1}) (5)	V_w (km s^{-1}) (6)	R.V. (km s^{-1}) (7)
HDE 236894......	130°82, -3°48	O8V[a]	3.1 ± 0.8	(0.3)	(1800)	-30[b]
HILT 23	132°93, -1°38	O9V[a]	2.1 ± 0.5	(0.1)	(1400)	
HD 13022.........	132°90, -2°58	O9.5II-III((n))[c]	2.8 ± 0.7	(0.4)	(1500)	-62[d]
HD 12323.........	132°92, -5°87	ON9V[c]	3.3 ± 0.8	0.004[e]	1175[f]	-96[g], -51[b]
HD 12993.........	133°11, -3°40	O6.5V[c]	2.9 ± 0.7	0.4[h]	2335[f]	-141[i], -122[g] -87[b]
HD 13338.........	133°52, -3°27	O9.5V[d]	2.1 ± 0.5	(0.1)	(1500)	
HD 13268.........	133°95, -5°00	ON8V[c]	1.9 ± 0.5	0.7[h]	2140[f]	-132[i], -128[b] -120[g]
HD 14442.........	134°20, -1°32	O5n(f)p[c]	2.9 ± 0.7	(3.0)	(2300)	-50[b], -48[g, j]
HD 13745.........	134°58, -4°95	O9.7II((n))[c]	2.5 ± 0.6	0.5[h]	1905[f]	-36[i], -27[d]
HD 14947.........	134°98, -1°77	O5If+[c]	2.6 ± 0.6	3.0 ± 0.7[k] 4.8 ± 2[l] <18[l] 7.5[n]	1885[f] 2300[m] 2350[n]	-86[g], -58[i] -48[j]
HD 14434.........	135°07, -3°82	O5.5Vn((f))p[o]	2.7 ± 0.7	≤ 0.7[e]	1960[f]	-33[b], -25[i] -47[g]
HD 15642.........	137°07, -4°73	O9.5III:n[c]	3.6 ± 0.9	(0.4)	1435[f]	-51[i]
HDE 237019......	137°42, -1°07	O8V[a]	2.4 ± 0.4	(0.3)	(1800)	-25[b]
HD 16691.........	137°72, -2°73	O4If+[c]	3.4 ± 0.9	7[h] 18	(2300)	-114[g], -46[d]
HD 16832.........	138°00, -2°88	O9.5II[c]	2.6 ± 0.7	(0.4)	(1500)	

REFERENCES.—(a) Mathys 1989; (b) Kendall et al. 1995; (c) Walborn 1973; (d) Cruz-Gonzalez et al. 1974; (e) Chlebowsky & Garmany 1991; (f) Howarth et al. 1997; (g) Conti et al. 1977; (h) Leitherer 1988; (i) McLachlan & Nandy 1985; (j) Underhill & Gilroy 1990; (k) Scuderi et al. 1998; (l) Lamers & Leitherer 1993; (m) Groenewegen & Lamers 1989; (n) Puls et al. 1996; (o) Walborn 1972.

TABLE 2

PARAMETERS OF THE 21 CM LINE OBSERVATIONS

Parameter	Value
Main beam efficiency	0.72
Beam size FWHM (arcmin)	9
Surveyed area	$132°\!.5 \leq l \leq 139°\!.0$
	$-4°\!.0 \leq b \leq +0°\!.2$
Total bandwidth (MHz)	3.125
Velocity range (km s^{-1})	$-430, +230$
Velocity resolution (km s^{-1})	1.3
Integration time per point (s)	31
Effective integration time (s)	63

Kalberla, Mebold, & Reif 1982). All profiles were corrected for stray radiation using the procedure developed by Kalberla, Mebold, & Reich (1980). To increase the signal-to-noise ratio we have averaged both polarizations. The final rms-noise temperature is about 0.14 K.

In order to investigate the large scale H I gas distribution in the environs of the Per OB1 association, complementary H I data were taken from the Leiden Dwingeloo H I Survey by Hartman & Burton (1997). This survey, obtained with the Dwingeloo radio telescope, covers a regular grid of $0°\!.5$ both in l and b, with a HPBW of $0°\!.6$, sampled at 1.03 km s^{-1}. The rms noise is about 0.07 K in brightness temperature.

Additional data sets were collected from other sources. To analyze the distribution of the ionized gas in the region we used the radio continuum survey at 2.7 GHz obtained with an angular resolution of $4'\!.3$ (Fürst et al. 1990).[2] The distribution of the molecular material was investigated using the FCRAO CO Survey of the Outer Galaxy (Heyer et al. 1998) available at the NASA ADC. The HPBW of this survey is 45″ sampled every 22″. The velocity ranges from -153 to $+40$ km s^{-1} sampled every 0.81 km s^{-1} with a velocity resolution of 0.98 km s^{-1}. The dust emission distribution was analyzed through *IRAS* images (angular resolution $\approx 6'$) available at the NASA ADC.

3. THE LARGE SCALE H I DISTRIBUTION IN THE REGION OF PER OB1

To facilitate the analysis of the H I emission distribution, in Figure 1 we show the average H I 21 cm line spectrum for the region $133°\!.0 \leq l \leq 138°\!.0$, $-3°\!.5 \leq b \leq 0°\!.0$ obtained from the Effelsberg observations. The profile displays the velocity interval -110 to $+20$ km s^{-1} where significant emission is detected.

The H I spectrum shows three main components. H I emission that peaks near $v \simeq -4$ km s^{-1} is associated with the local spiral arm at distances $d_k \leq 1.5$–2 kpc. The component that peaks at $v \simeq -45$ km s^{-1} appears related to the Perseus spiral arm at $d_k \simeq 2.0$–7 kpc (e.g., Caswell & Haynes 1987); while the features with velocities $v \leq -75$ km s^{-1} would correspond to the Cygnus spiral arm (Kimeswenger & Weinberger 1989) at $d_k \geq 10$ kpc. The kinematical distances were estimated from the analytical fit to the rotation curve obtained by Brand & Blitz (1993).

To investigate the neutral gas distribution around Per OB1, we examined the H I emission in the region $128°\!.0 \leq$

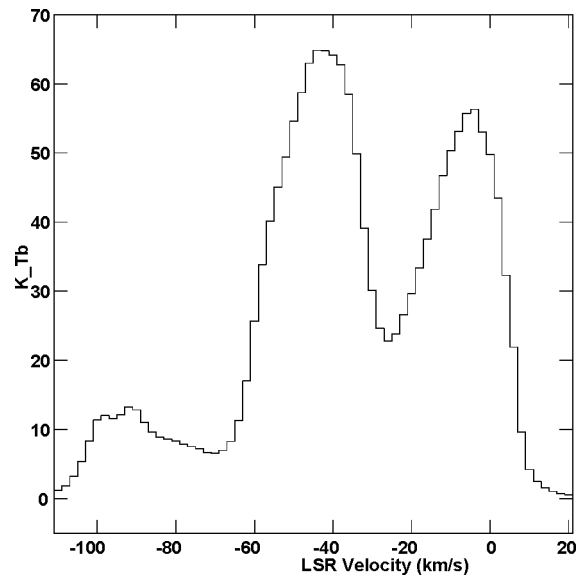FIG. 1.—Average H I profile obtained from the Effelsberg observations through the region $133°\!.0 \leq l \leq 138°\!.0$, $-3°\!.5 \leq b \leq 0°\!.0$.

$l \leq 142°\!.0$, $-17°\!.0 \leq b \leq +1°\!.0$. The left panel of Figure 2 illustrates the neutral hydrogen column density distribution $N_{\rm H\,I}$ within the velocity range -32 to -20 km s^{-1}, under the assumption of optically thin emission, obtained from the low angular resolution H I survey. The O and B stars belonging to Per OB1 are indicated as asterisks and plus signs, respectively. The circles mark the position of the open clusters h and χ Persei. For the sake of clarity, only the position of the O-type star HD 14434 is shown in this region.

The map shows a region of low emission centered at $(l, b) = (134°\!.5, -2°\!.5)$, of about 6° in size. Since it is detected within the velocity range -32 to -20 km s^{-1}, we adopt the mean velocity in the interval $(-26$ km s$^{-1})$ as the systemic velocity $v_{\rm sys}$. The application of a flat galactic rotation curve (Brand & Blitz 1993) predicts that gas with $v_{\rm sys}$ should be located at a kinematic distance $d_k \simeq 2.5$ kpc. Their Figures $2a$ and $2b$, which include noncircular motions, indicate $d_k \simeq 1.8$ kpc for the same velocity. These values are in agreement with the optical distance to Per OB1 (2.3 kpc; see § 1), suggesting that the H I feature may be related to Per OB1.

The H I low-emission region appears to be excavated in the gas layer. It is partially encircled by enhanced emission regions seen at $l \approx 132°\!.5$, from $b \approx -4°\!.0$ to 0°; $b = 0°$ from $l \approx 133°\!.0$ to $136°\!.0$ and from $(l, b) = (136°\!.0, 0°)$ to $(l, b) = (139°\!.0, -4°\!.0)$. The contour lines seem to be piled up mainly at $b = 0°$ from $l = 133°\!.0$ to $135°\!.0$, and $l = 132°\!.5$ from $b = -3°\!.0$ to $-1°\!.0$, suggesting that the neutral gas is compressed. Contrariwise, a smooth gradient is present at $l = 136°$. This structure can be identified with the H I shell candidate described by Heiles (1979) and related to Per OB1. Note that most of the early-type stars in the association appear projected onto the low-emission region or onto their borders. Thus, the spatial coincidence between the H I low-emission region and Per OB1, suggests that the OB association is interacting with its environs and that the low-emission region and the surrounding envelope may be the result of such interaction. We can derive an upper limit of 10 km s^{-1} for the expansion velocity of this structure.
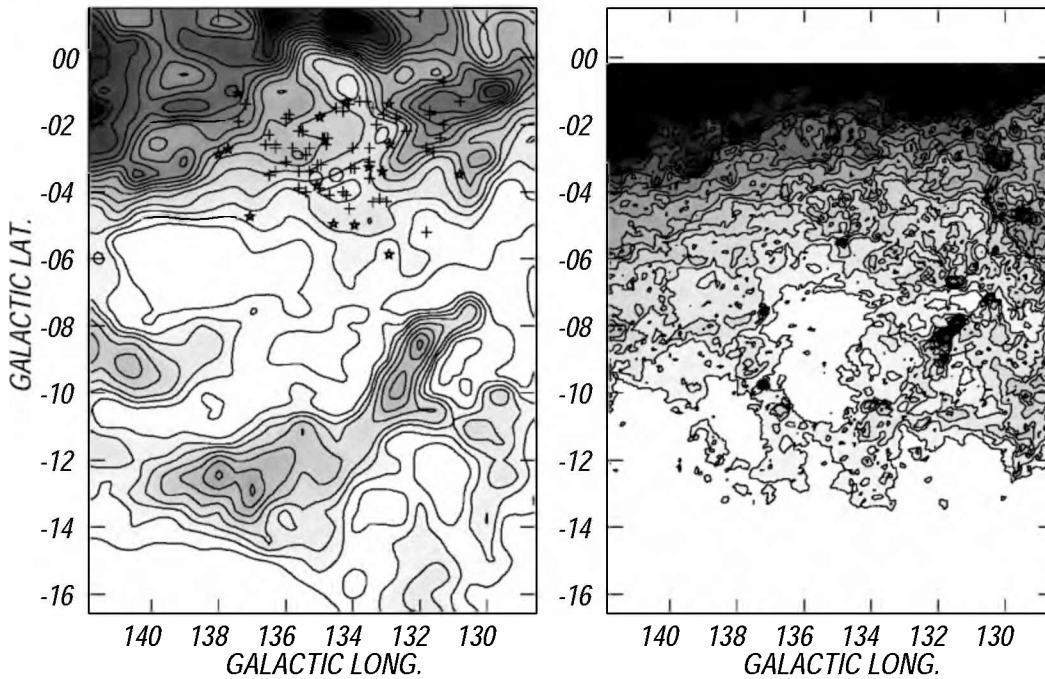
Fig. 2.—*Left panel*: Latitude-longitude H I column density image through the velocity range -32 to -20 km s^{-1}, obtained from the Hartman & Burton survey, showing the H I gas distribution in the vicinity of Per OB1. The gray scale corresponds to $(1.7-12.5) \times 10^{20}$ cm^{-2}. The contour levels are 1.5, 2.0, 2.5, 3.0, 3.8, 4.6, 5.4, 6.2, 7.0, 7.8, 8.6, 9.4, 10.2, 11.0, and 11.8 $\times 10^{20}$ cm^{-2}. The position of the O-type stars belonging to Per OB1 is indicated with stars, while the B0–B5 type stars are shown as plus signs. The small circles near $b = -4°$ mark the position of the open clusters. *Right panel*: *IRAS* image at 100 μm. The gray scale corresponds to 9–45 MJy sr^{-1}. The contour levels are 10, 12, 14, 16, 18, 20, 22, 25, 28, 31, 34, 37, and 40 MJy sr^{-1}.

The figure also illustrates the presence of strong H I emission between $-14° \leq b \leq -8°$, where the brighter H I clouds define an arclike feature. An inspection of the H I maps at different velocities shows the presence of strong H I emission at $-18° \leq b \leq -8°$, within the velocity interval -55 to -18 km s^{-1}, which would be related to the Perseus spiral arm. The large arclike feature at $(l, b) = (134°0, -12°0)$ is clearly detected within the velocity interval -33 to -20 km s^{-1}. Part of this feature can be identified with the worm candidate GS132.6-9. The brightness of the arclike feature vanishes toward higher negative velocities until it disappears at $\simeq -39$ km s^{-1}. We believe that the arclike structure also conforms the H I shell related to Per OB1.

The *IRAS* image at 100 μm (Fig. 2, *right panel*) reveals infrared emission following the inner border of the large H I arclike feature. Slightly enhanced IR emission also delineates the section of the H I shell seen at $l \geq 137°0$, from $b = -9°5$ to $-5°0$. Enhanced IR emission is also present at $(l, b) = (137°0, -10°0)$, where little H I is detected. Thus, an IR counterpart can be identified in the region of the shell toward higher negative Galactic latitudes. The IR counterpart of the region of the H I shell closer to the galactic plane is more difficult to distinguish. It may be masked by the bulk of the galactic contribution.

The radio continuum emission distribution at 1408 MHz (Reich et al. 1990) displays a region of low emission coincident with the large cavity seen in the *IRAS* and H I images near $(l, b) = (135°0, -8°5)$. A relatively small emission region at $(l, b) = (131°5, -8°3)$, which correlates with the brightest region of the H I arclike feature, is also observed.

Adopting for the H I shell the optical distance to Per OB1, the angular and linear radius of the upper part of the shell (i.e., the region closer to the galactic plane) is $\simeq 3°0$ or

110 pc. By including the arclike feature and the emission seen near $(l, b) = (141°0, -9°)$, the shell related to Per OB1 is $9° \times 14°$ or 350×550 pc in size (which corresponds to a mean radius of 220 pc). The uncertainty in size is 20%, assuming an error of 20% in the distance to Per OB1.

The neutral masses in both regions of the shell were evaluated separately. We estimated the swept-up mass in the upper part of the shell M_s from mean $N_{H I}$-values in the low-emission region and in their surroundings and adopted the swept-up mass to be a mean value between them. We found $M_s \simeq 3.7 \times 10^4\ M_\odot$. A helium abundance of 10% was assumed. The mass content in the lower part of the shell is about $5.1 \times 10^4\ M_\odot$. These masses are lower limits since we have taken into account the neutral mass only. By distributing $8.8 \times 10^4\ M_\odot$ uniformly within a sphere of 220 pc in radius, the ambient gas density results ~ 0.1 cm^{-3}. The error in the derived masses is about 40%.

No H II region was cataloged within the area of Per OB1. A radio recombination line was detected at $l = 132°16$, $b = -0°73$, at $v_{LSR} = -56.6$ km s^{-1} (Lockman 1989). This region is projected onto the border of the H I shell and is located at a kinematic distance of 5–6 kpc. Because of its position and distance, we assume it is unrelated to Per OB1.

4. H I BUBBLES SURROUNDING MASSIVE STARS

To investigate the H I gas distribution in the environs of the O and Of stars in the association we used the H I data obtained at Effelsberg. H I cavities and shells candidates to be related to the individual stars in the association were carefully searched for in a series of (l, b) maps constructed in steps of 2 km s^{-1}, showing brightness temperature at constant velocity. We have discovered H I structures probably associated with the Of stars HD 14947, 14442, and 16691, with the O stars HD 13022 and HD 13338, and with the B

stars HD 15233 and Hilt 311. In all cases, the location of the stars within the H I cavities or on their borders and the agreement between the kinematic distance to the features and the optical distance derived for Per OB1 indicate an association between the H I structure and the star.

The structures are partially seen in Figure 3, which displays the H I gas distribution within the same velocity interval as Figure 2, as obtained using the Effelsberg H I data. The image shows the same large-scale feature as Figure 2 (*left panel*) and a large number of small-scale H I structures with some of the massive stars in the association projected onto small H I voids.

The main physical parameters of the H I structures are listed in Table 3. The velocity interval v_1, v_2 corresponds to the velocity range in which each H I feature is clearly identified and is usually larger than the velocity range where the column density image was obtained. The systemic velocity v_{sys} of each shell was used to derive its kinematic distance d_k. Since, within errors, d_k agrees in all cases with the distance to Per OB1, we adopted the optical distance to the association (2.3 kpc) in our calculations, instead of the kinematic distances to the H I structures or the stellar distances. The radius R_s of each structure was obtained as a mean value between the radii of the void (R_v) and the envelope (R_{env}),
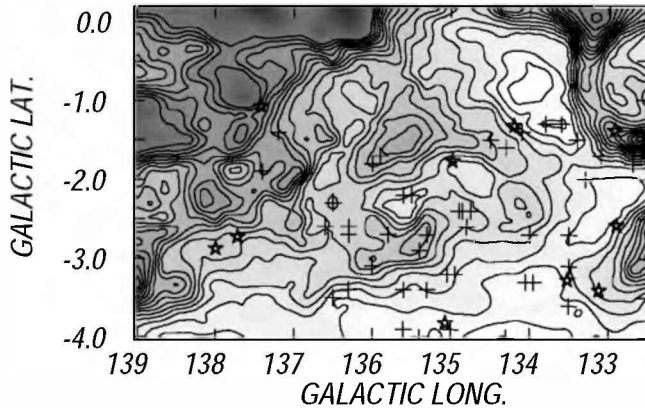

FIG. 3.—Same as Fig. 2, as obtained from the Effelsberg data. The gray scale corresponds to $(2.4–13.6) \times 10^{20}$ cm^{-2}. The contour levels are 2.0, 2.5, 3.0, 3.5, 4.0, 4.5, 5.0, 5.5, 6.0, 6.5, 7.0, 7.5, 8.0, 8.5, 9.0, 9.5, and 10.0×10^{20} cm^{-2}. The star and plus signs have the same meaning as in Fig. 2.

and corresponds approximately to the radius defined by the position of the maxima in the shell. The major and minor semiaxis ($r_M \times r_m$) are given for cases of noncircular cavities and shells. The neutral masses were evaluated assuming the optically thin case and a typical interstellar helium abundance of 10%. The swept-up neutral masses M_s were obtained as mean values between the neutral mass deficiency in the voids M_{def} and the mass in the envelopes M_{env}. As in previous papers, ambient densities were evaluated by distributing M_s over the volume of the bubbles. The expansion velocities were derived as $(v_1 - v_2)/2 + 2$ km s^{-1}. Swept-up masses and expansion velocities were used to estimate the kinetic energies of the neutral shells.

The uncertainty in v_{sys}, which is 2 km s^{-1}, arises in the velocity interval between the individual maps in the series; while the uncertainty in d_k originates in the presence of noncircular motions of about ± 7 km s^{-1} (Burton 1988). The major source of error in radii, masses and kinetic energies originates in the distance uncertainty. An error of 20% in the distance to Per OB1 (see § 1) implies 20% error in radius and 40% error in the derived masses. The uncertainty in the kinetic energy is at least 45%.

In the following sections we briefly describe the discovered H I bubbles.

4.1. *The ISM in the Vicinity of HD 14442* [O5n(f)p]

The top panel of Figure 4 displays the H I column density distribution within the velocity interval -28 to -18 km s^{-1} in the neighborhood of HD 14442. The O5n(f) star, indicated by a star, appears projected close to the borders of a large and complex H I cavity centered at $(l, b) = (134.1, -0.9)$. The cavity contains two minima, centered at $(l, b) = (134.0, -0.9)$ and $(l, b) = (134.4, -0.5)$. The surrounding envelope is clearly detected toward the southern border of the cavity ($b = -1.7$). Toward $l \approx 133.25$, the H I envelope may be masked by the presence of a H I filament probably unrelated to the O-type star. The existence of a H I shell bordering the cavity near $l \approx 135.0$ cannot be confirmed from the present data. The portion of the H I shell toward $b = -0.25$, which is barely visible, separates the double-minima structure from a smaller cavity detected at $(l, b) = (135.2, -0.0)$.

Adopting the mean value of the velocity interval in which the H I feature is seen as the systemic velocity $v_{sys} = -23$ km s^{-1}, we derived a kinematic distance of $\simeq 2.2$ kpc, in

TABLE 3

PARAMETERS OF THE H I STRUCTURES SURROUNDING MASSIVE STARS

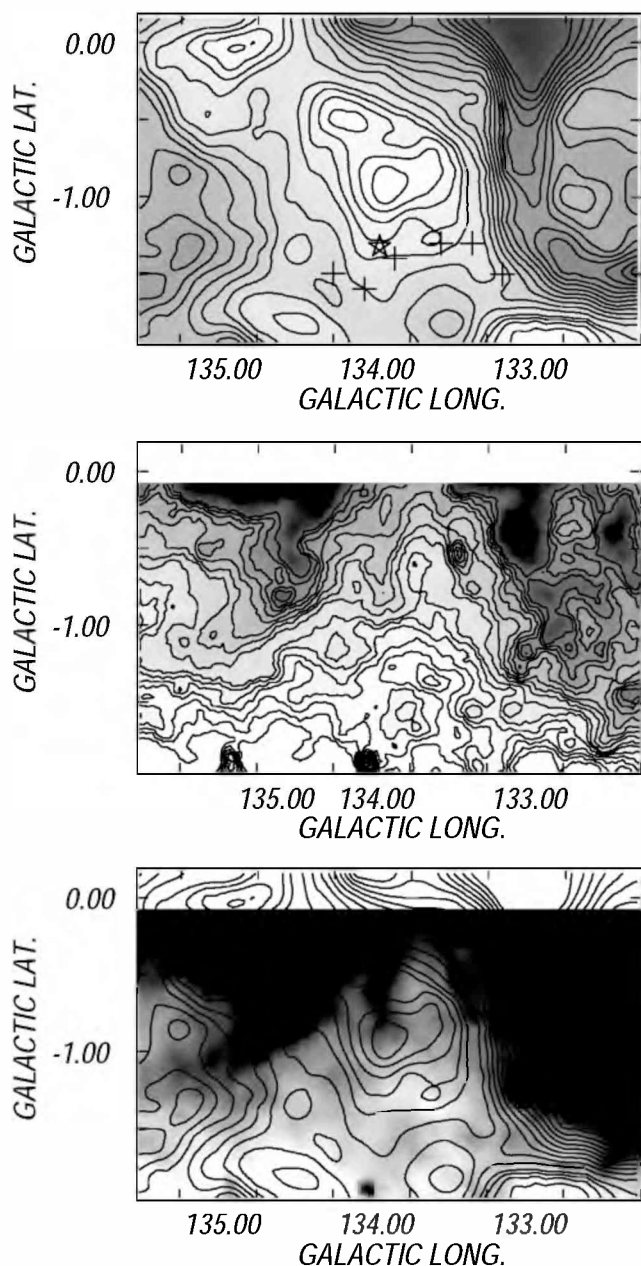| Star	HD 14442	HD 14947	HD 16691	HD13022	HD13338	HD15233 Hilt 311
(l, b) center	134.1, -0.9	134.7, -1.8	137.65, -3.15	133.15, -2.25	133.75, -3.3	135.6, -2.3
Vel. interval v_1, v_2 (km s^{-1})	$-32, -18$	$-30, -14$	$-32, -20$	$-38, -14$	$-26, -16$	$-32, -16$
Systemic vel. v_{sys} (km s^{-1})	-23	-22	-25	-22	-21	-22
Kinematic distance d_k (kpc)	2.2	2.1	2.4	2.1	2.0	2.1
Radius of the cavity (pc)	30×18	16×8	26×15	22×15	15	12
Radius of the envelope (pc)	40	30×20	37×25	...	22	24
Mean radius R_s (pc)	35×30	24×14	31×20	22×29	18	18
M_{def} ($M_\odot$)	920	180	620	1100	240	220
M_{env} ($M_\odot$)	4060	1900	1660	...	700	1300
M_s ($M_\odot$)	2500	1040	1140	1100	470	750
n (cm^{-3})	0.8	1.8	1.0	1.4	0.8	1.3
V_{exp} (km s^{-1})	9	10	8	14	7	10
E_k (10^{48} ergs)	2.0	1.0	0.7	≥ 1.6	0.3	0.8

FIG. 4.—*Top panel*: Latitude-longitude H I column density image through the velocity range −28 to −18 km s⁻¹, showing the H I gas distribution in the vicinity of HD 14442. The gray scale corresponds to $(2.2–9.5) \times 10^{20}$ cm⁻². The contour levels are 1.8, 2.0 2.2, 2.4, 2.6, 2.8, 3.0, 3.4, 3.8, 4.2, 4.6, 5.0, 5.4, 5.8, 6.2, 6.6, 7.0, 7.4, 7.8, and 8.2 × 10²⁰ cm⁻². The star indicates the position of HD 14442, while the plus signs mark the position of other early-type stars (see § 5). *Middle panel*: IR image at 100 μm. The gray scale corresponds to 40 to 120 MJy sr⁻¹ and the contour lines are 36, 38, 40, 42, 44, 46, 48, 52, 56, 60, 66, 72, 78, 84, and 90 MJy/sr. *Bottom panel*: Overlay of the same H I contour lines and a gray-scale *IRAS* image. The gray scale corresponds to 36 to 60 MJy sr⁻¹.

agreement with the optical distance to Per OB1 and with the stellar distance.

The middle panel of Figure 4 presents the *IRAS* infrared emission at 100 μm, while the bottom panel displays an overlay of the IR (*gray scale*) and H I (*contour lines*) images. The H I minimum at $(l, b) = (134°4, −0°5)$ appears projected onto a region of relatively low IR emission delineated by enhanced IR emission toward $b = −0°5$ and $l = 134°5$. The strong IR emission detected toward $l = 133°0$ is discon-

nected to the cavity. The lowest IR emission region is detected near $(l, b) = (133°8, −1°35)$, projected onto a small region of the H I minimum at $b = −0°9$. The lack of a clear IR shell might be due to the presence of a galactic IR gradient and confusion effects originated in the fact that IR emission prevents discrimination of material at different velocities.

Very faint Hα + [N II] emission (Parker, Gull, & Kirschner 1979) is seen projected onto part of the H I cavity, suggesting the presence of low density ionized gas. The radio continuum emission at 2.7 GHz (Fürst et al. 1990) is quite complex in this region. An area of low emission centered at the position of the lowest IR emission region described before is clearly visible. No CO emission was detected within the velocity range where the H I structure is present.

The distribution of material in the surroundings of the Of star supports the idea that this material could have been swept-up by the action of the strong stellar winds of the star. Both radio continuum and IR observations suggest that only the H I cavity with the highest negative galactic latitude could have been blown by the Of star.

The plus signs in Figure 4 mark the position of the early-type stars belonging to Per OB1 which are projected onto the borders of the H I cavity, namely BD + 59° 451 (B1II), BD + 59° 456 (B0.5V), BD + 59° 461 (B1II), BD + 58° 451 (B1III), BD + 58° 453 (B1V), and HDE236960 (B0.5III). Their contribution in shaping the cavity will be analyzed in § 5.

4.2. *The ISM surrounding HD 14947* [*O5If+*]

The H I column density distribution within the velocity interval −28 to −14 km s⁻¹ in the vicinity of the O5f+ star is illustrated in the top panel of Figure 5. An elongated cavity, centered at $(l, b) = (134°7, −1°8)$ is clearly seen in the image. HD 14947, indicated by a star symbol, appears projected within the cavity, close to one of its higher density borders. The void is encircled by an almost complete and thick shell. An inspection of the H I images at full velocity resolution shows that as the velocity changes, the position of the center of the H I structure varies, indicating a distorted feature. Within the velocity interval −30 to −22 km s⁻¹ the minimum is centered at $(l, b) = (134°7, −2°0)$, while within the velocity interval −22 to −14 km s⁻¹, it is centered at $(l, b) = (134°7, −1°7)$. Adopting a systemic velocity $v_{sys} = −22$ km s⁻¹, the kinematic distance turns out to be 2.1 kpc, in very good agreement with the distance to Per OB1 as well as with the stellar distance.

The location of HD 14947 close to one of the higher density borders of the cavity together with the agreement between the kinematic distance of the structure and the stellar distance suggest a physical association between the H I structure and the Of star. No other massive star belonging to the association appears within the void or onto its borders.

The bottom panel of Figure 5 displays the same H I contours superposed to a gray-scale representation of the *IRAS* image at 100 μm. The image reveals a low IR emission region, which coincides with the H I cavity and is surrounded by an open ringlike feature opposite the galactic plane.

An inspection of the radio continuum image at 2.7 GHz reveals the presence of weak diffuse emission within the region of the cavity. However, it is not clear if it is related to
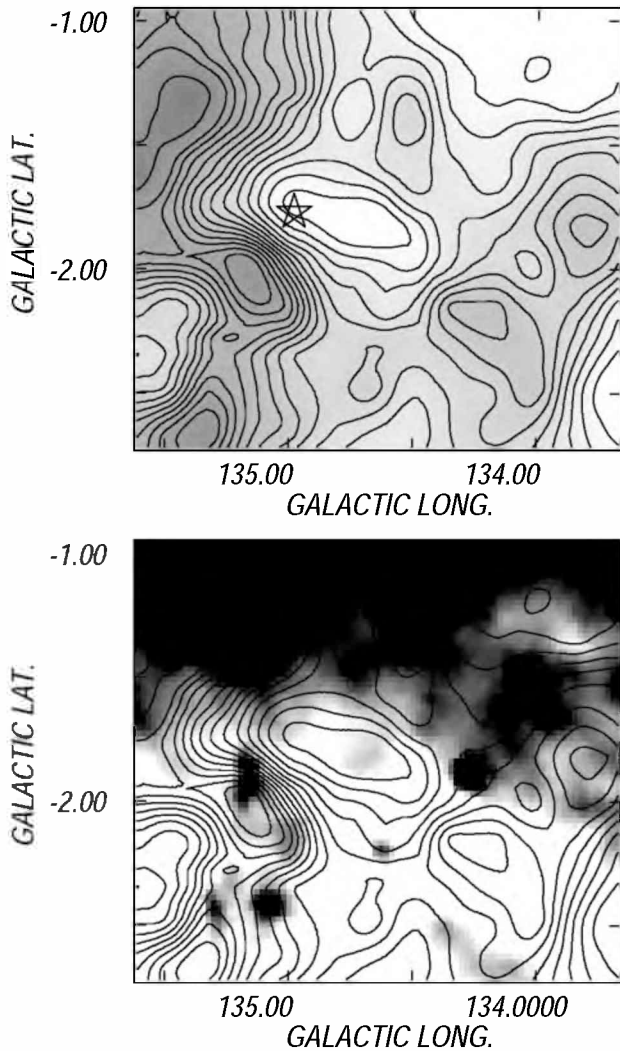
FIG. 5.—*Top panel*: Latitude-longitude H I column density image through the velocity range -28 to -14 km s^{-1}, showing the H I gas distribution in the vicinity of HD 14947. The gray scale corresponds to $(3.3\text{–}6.5) \times 10^{20}$ cm^{-2}. The contour levels are 3.4, 3.6, 3.8, 4.0, 4.2, 4.4, 4.6, 4.8, 5.0, 5.2, 5.4, 5.6, 5.8, 6.0, 6.2, 6.6, and 7.0×10^{20} cm^{-2}. The star indicates the position of HD 14947. *Bottom panel*: Overlay of the same H I contour lines and a gray-scale *IRAS* image at 100 μm. The gray scale corresponds to 35–42 MJy sr^{-1}.

the H I structure. The analysis of the molecular data in the region does not show molecular material associated with the detected H I shell.

As for the case of HD 14442, these results support the idea of a wind-blown bubble origin for the H I structure linked to HD 14947.

4.3. *The ISM in the Vicinity of HD 16691* [*O4If+*]

The top panel of Figure 6 displays the H I column density distribution around HD 16691, within the velocity interval -28 to -22 km s^{-1}. The image shows a low-emission region centered at $(l, b) = (137°65, -3°15)$. It appears open opposite to the galactic plane, probably showing the effects of the galactic density gradient. The O4If+ star, indicated as a star symbol, is located close to one of the high density borders of the feature. The brightest portions of the shell are detected toward the galactic plane and toward the higher galactic longitude border. Assuming $v_{\rm sys} = -25$ km s^{-1}, a
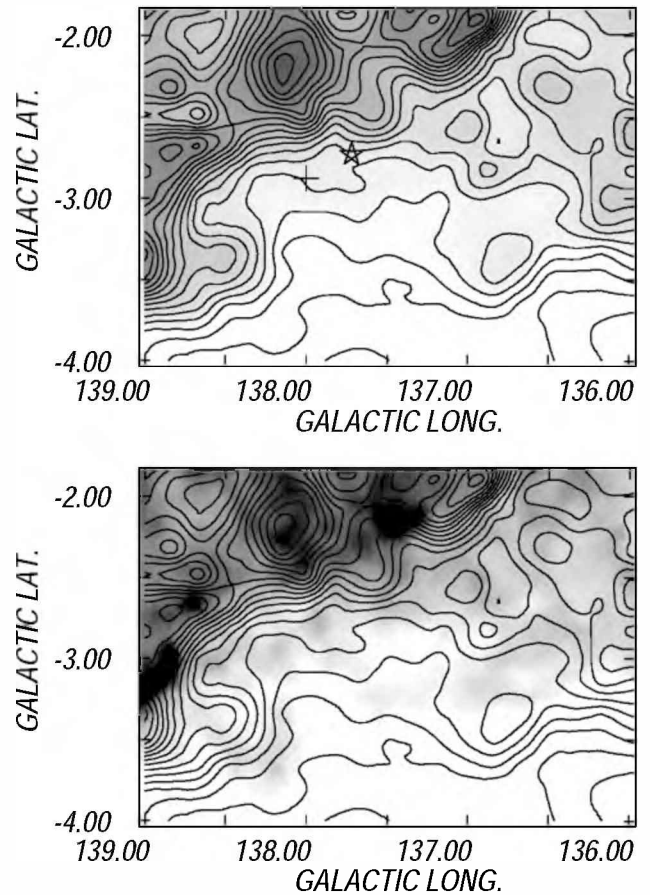
FIG. 6.—*Top panel*: Latitude-longitude H I column density image through the velocity range -28 to -22 km s^{-1}, showing the H I gas distribution in the vicinity of HD 16691. The gray scale corresponds to $(1.8\text{–}4.8) \times 10^{20}$ cm^{-2}. The contour levels are from 1.1 to 4.7×10^{20} cm^{-2} in steps of 0.2×10^{20} cm^{-2}. The star indicates the position of HD 16691, while the plus sign marks the position of HD 16832 (see § 5). *Bottom panel*: Overlay of the same H I contour lines and a gray scale *IRAS* image at 100 μm. The gray scale corresponds to 28–50 MJy sr^{-1}.

kinematic distance of about 2.4 kpc is derived, in agreement with the distance to Per OB1. The cross marks the position of the O9.5II star HD 16832 (see Table 1). According to its location, it might also contribute to the formation of the cavity.

The bottom panel of Figure 6 shows the superposition of the 100 μm *IRAS* image (*gray scale*) and the H I emission (*contour lines*). A clear IR counterpart is detected. The radio continuum emission at 2.7 GHz, which is very faint in this area, displays a low-emission region which partially correlates with the H I cavity. No CO emission was found to be associated with this structure.

In this case, the evidence of the presence of an H I structure related to the star is less conclusive than in the other cases. However, we note that similar H I distributions have been found for some H I bubbles associated with WR stars (see Arnal et al. 1999).

4.4. *The ISM in the Vicinity of HD 13022* [*O9.5II-III((n))*] *and HD 13338* [*O9.5V*]

The neutral gas distribution in the vicinity of these O-type stars is shown in Figure 7, where we display the $N_{\rm H\,I}$ within the velocity interval -24 to -16 km s^{-1}. HD 13022
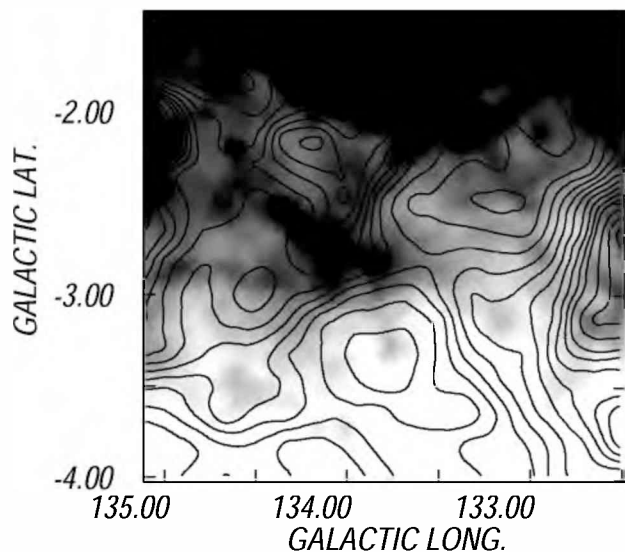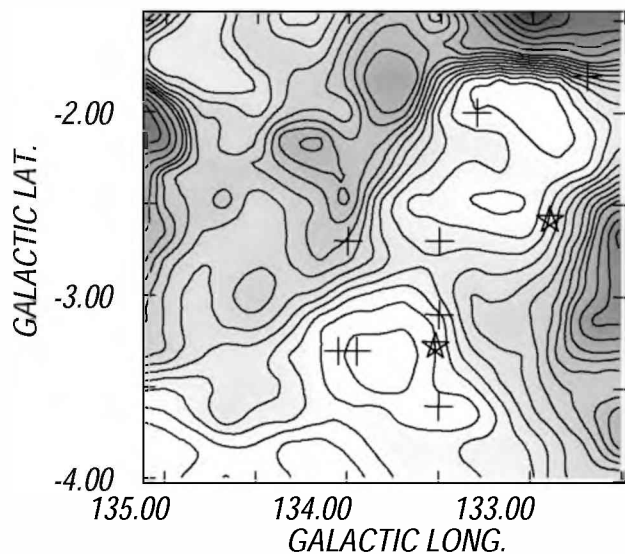
FIG. 7.—*Top panel*: Latitude-longitude H I column density image through the velocity range -24 to -16 km s^{-1}, showing the H I gas distribution in the vicinity of HD 13022 and HD 13338. The gray scale corresponds to $(1.8-6.2) \times 10^{20}$ cm^{-2}. The contour levels are 1.8, 2.0 2.2, 2.4, 2.6, 2.8, 3.0, 3.2, 3.4, 3.6, 3.8, 4.2, 4.6, 5.0, 5.4, and 5.8×10^{20} cm^{-2}. The stars mark the position of HD 13022 and HD 13338, while the plus signs indicate the position of the other early-type stars (see § 5). *Bottom panel*: Overlay of the same H I contour lines and a gray scale *IRAS* image at 100 μm. The gray scale corresponds to 22–35 MJy sr^{-1}.
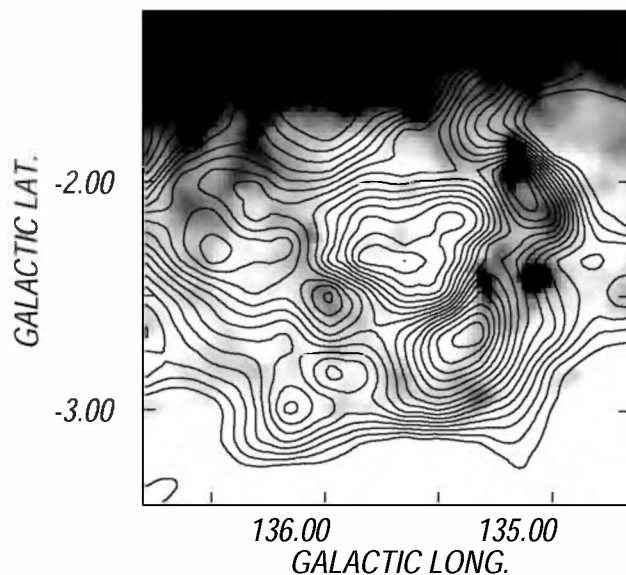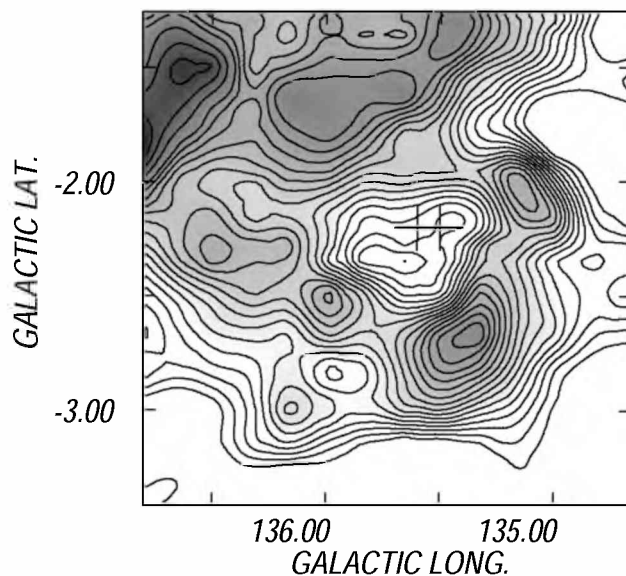
FIG. 8.—*Top panel*: Latitude-longitude H I column density image through the velocity range -28 to -18 km s^{-1}, showing the H I gas distribution in the vicinity of HD 15233 and Hilt 233. The gray scale corresponds to $(5-8.5) \times 10^{20}$ cm^{-2}. The contour levels are 4.2, 4.4, 4.6, 4.8, 5.0, 5.2, 5.4, 5.6, 5.8, 6.0, 6.2, 6.4, 6.6, 6.8, 7.0, 7.4, 7.8, and 8.2×10^{20} cm^{-2}. The stars indicate the position of HD 15233 and Hilt 233. *Bottom panel*: Overlay of the same H I contour lines and a gray-scale *IRAS* image at 100 μm. The gray scale corresponds to 32–40 MJy sr^{-1}.

and HD 13338, indicated as star symbols, appear projected close to the borders of the H I cavities centered at $(l, b) =$ $(133°15, -2°25)$ and $(l, b) = (133°75, -3°3)$, respectively. The location of the stars and the kinematic distances derived for the features enable us to associate the H I structures with the O-type stars.

The structure close to HD 13022 displays two small H I minima. The whole feature is surrounded by neutral clouds toward $l \simeq 133°75$; but due to the location of the structure close to the border of the surveyed region, the presence of an envelope toward $l = 132°5$ cannot be confirmed. Consequently, masses and densities were estimated from the mass deficiency in the whole cavity. Three massive stars might also be related to this cavity: HD 13036 (B0.5III), HDE 236954 (B3Ib), and BD + 57°520 (B1II).

The H I envelope surrounding the void connected to HD 13338 is barely discernible. According to the extension in velocity and systemic velocity, this structure is expanding asymmetrically. Additional early-type stars that can be associated with the structure are HD 13267 (B5Ia), HD 13716 (B0.5III), HD 13758 (B0.5IV), and BD + 57°513 (B1III).

The IR emission at 100 μm delineates the borders of the structure related to HD 13338 toward larger galactic longitudes and the galactic plane. No clear correlation between H I and IR emission is apparent for the structure related to HD 13022. Both H I structures are projected onto a region with low radio continuum emission. The cavity closer to the galactic plane appears partially surrounded by enhanced

radio emission. No CO emission was detected in connection with these features.

4.5. The ISM in the Vicinity of the B1III-Type Stars HD 15233 and Hilt 311

The top panel of Figure 8 shows the distribution of $N_{\rm H\,I}$ in the vicinity of HD 15233 and Hilt 311 obtained within the velocity interval -28 to -16 km s^{-1}. The image shows a rather circular cavity centered at $(l, b) = (135°6, -2°2)$, encompassed by a well-defined almost complete shell. The structure presents its largest dimensions and its highest temperature gradient at -22 km s^{-1}, and we adopted this value as the systemic velocity. Since the H I feature is detected within the velocity interval -32 to -16 km s^{-1}, this systemic velocity suggests the structure is expanding asymmetrically: while the approaching part of the shell expands at 12 km s^{-1}, the receding part moves at 8 km s^{-1}.

Circular galactic rotation models predict kinematic distances of about 2.2 kpc for this velocity, in close agreement with the distance to Per OB1. Two stars belonging to the association appear located within the cavity: HD 15233 $[(l, b) = (135°6, -2°2)]$ and Hilt 311 $[(l, b) = (135°5, -2°2)]$ (Garmany & Stencel 1992), classified as B1III. Their position, close to the center of the void, is marked with crosses in the figure.

As for the other features, the bottom panel of the figure shows the distribution of $N_{\rm H\,I}$ (contour lines) superposed to the IRAS emission at 100 μm. A clear IR counterpart is seen. The radio continuum map at 2.7 GHz shows a low-emission region that correlates with the H I void. Based on both morphological and kinematic arguments, the CO emission detected within the velocity interval -15 to -13.5 km s^{-1} may be related to the H I shell. Thus, the bulk of the observational data discussed here indicate that there is a lack of neutral and ionized gas within the structure.

5. DISCUSSION

5.1. The Origin and Energetics of the Structures

In order to test if the features surrounding the massive stars can be originated by stellar winds, we have evaluated the mechanical energy E_w released into the ISM for the massive stars during the dynamical age t_d of the bubbles $(E_w = L_w t_d = \dot{M}V_w^2 t_d/2)$. The results are summarized in Table 4. The dynamical ages were derived as $t_d = 0.55R_S/V_{\rm exp}$, where the constant represents a mean value between the energy and momentum conserving cases. The stellar wind luminosity L_{w-O} and the mechanical energy E_{w-O} were obtained separately for stars HD 14442, HD 14947, HD 16691, HD 13022, HD 13338, and HD 15233

and Hiltner 311. $E_{w-\rm other}$-values show the contribution of other massive stars that, according to their location, might contribute in the formation of the structures (indicated as plus signs in the $N_{\rm H\,I}$ figures). The mass-loss rates for these stars were estimated from the expression by Lamers & Leitherer (1993), while the terminal velocities correspond to mean values (Prinja et al. 1990). Errors in dynamical ages and mechanical energies are typically 45% and 70%, respectively.

The fifth and sixth rows of Table 4 show the energy and momentum conversion efficiencies (see Treffers & Chu 1982). ϵ was evaluated as the ratio between the kinetic energy of the neutral structures E_k and the mechanical energy provided by all the massive stars in each region $(E_{w-O} + E_{w-\rm other})$; while π measures the ratio of the outward momentum of the shell $(M_s V_{\rm exp})$ to the integrated momentum carried by the stellar wind of the same stars $(\dot{M}V_w t_d)$. Current models for the evolution of interstellar bubbles state $\epsilon \simeq 0.2$ and $\pi \geq 1$ for energy conserving stages and $\epsilon \ll 0.2$ and $\pi = 1$ for momentum conserving phases. The uncertainty in ϵ is about 100%.

Several conclusions can be drawn from the table. The dynamical ages t_d are, within errors, roughly compatible with the lifetime in the main sequence of massive stars (Schaerer et al. 1996). $\epsilon \leq 0.01$ for the three structures related to the Of stars HD 14442, HD 14947, and HD 16691. According to evolutionary models of WBBs (e.g., García-Segura & Mac Low 1995), these values indicate that the stars are capable of blowing the observed interstellar bubbles by means of the stellar wind mechanism. The comparison of E_{w-O} and $E_{w-\rm other}$ suggests that the three Of stars would be the main contributors to the formation of their own bubbles. Our results also suggest that the bubbles are in the momentum conserving case or in an intermediate stage between energy and momentum conserving cases.

For the bubbles associated with the late O stars HD 13022 and HD 13338, the contribution of other massive stars is important, being half the mechanical energy input in the case of HD 13022. The ϵ-values are in the range 0.16–0.02. Again in this case, the hypothesis of a stellar wind origin may be held. Within errors, these bubbles appear to be closer to the energy conserving case than the bubbles related to the Of stars.

The ϵ-value derived for the H I structure related to the two B stars, clearly indicates that this feature has been originated by a different mechanism since a stellar wind origin is difficult to support. Similar H I structures connected to supernova remnants have also been found; and a supernova explosion in Per OB1 cannot be ruled out. The origin of this H I feature will be analyzed elsewhere.

TABLE 4

DERIVED PARAMETERS

Star	HD 14442	HD 14947	HD 16691	HD13022	HD13338	HD15233 Hilt 311
L_{w-O} (10^{36} ergs s^{-1})	5.2	3.5–33	12–31	0.3	0.07	0.015
t_d (10^6 yr)	2.0	1.0	1.8	1.0	1.4	1.0
E_{w-O} (10^{50} ergs)	3.2	1–10	7–17	0.09	0.03	0.006
$E_{w-\rm other}$ (10^{50} ergs)	0.12	...	0.17	0.045	0.12	...
ϵ	0.006	0.01–0.001	0.001–0.0004	0.2–0.1	0.1–0.02	1.6
π	0.6	0.3–1.8	0.1–0.3	14	4	90
$C_{\rm ax}$	1.7	2.0	1.7	1.5	1.0	...
$C_{\rm off}$	0.5	0.7	0.6	0.6	0.3	...

The low ϵ-values derived for the new H I interstellar bubbles could also be explained if a substantial amount of the energy provided by the stars has released into the large H I structure related to Per OB1 as a whole. Although this leakage cannot be ruled out, we note that similar low values were found for most of the interstellar bubbles associated with Wolf-Rayet and Of stars (e.g., Treffers & Chu 1982; Wrigge 1999; Benaglia & Cappa 1999; Cappa et al. 1999, and references therein). As pointed out by García-Segura & Mac Low (1995) and Wrigge (1999) an overestimation of the stellar wind parameters for massive stars cannot be ruled out.

Finally, it is of interest to evaluate the energetics of the large H I shell related to Per OB1 as a whole. The kinetic energy E_k of the shell is $\approx 9 \times 10^{49}$ ergs. Taking into account that for an energy conserving bubble $E_k = 0.2$ E_{w-min}, E_{w-min} results $\simeq 4.5 \times 10^{50}$. E_{w-min} represents the minimum stellar wind mechanical energy necessary to blow the observed H I shell. At the same time, we estimated the energy E_w released into the ISM by all the B stars in the association through the stellar wind mechanism. Here, we take into account only the B stars since some of the O and Of stars have blown their own bubbles and the contribution of these stars to the energetics of the large H I shell is difficult to evaluate. Consequently, we believe that the derived E_w-value represents a lower limit to the stellar wind energy available to blow the large H I shell. $\dot{M}$ and V_w for the B stars were obtained using the fitting formula by Lamers & Leitherer (1993) and mean values by Prinja et al. (1990), respectively. Adopting the age of the shell to be 7×10^6 yr (see § 1), E_w turns out to be about 1.3×10^{51} ergs. Then $E_k/E_w \simeq 0.07$, indicating that Per OB1 suffices to blow the large H I shell.

5.2. Morphological Characteristics

We evaluated two parameters to characterize the morphology of the H I interstellar bubbles: the ratio of the major to the minor axis of the cavity $C_{ax} = 2r_M/2r_m$; and C_{off}, which is the ratio of the observed projected distance of the star responsible for creating the bubble from its center to the minor axis of the cavity (Arnal 1992). These parameters enable us to quantify the ellipticity of the H I interstellar bubbles and the eccentric location of the stars.

The values for C_{ax} and C_{off} are listed in Table 4. C_{ax} varies between 1.0 and 2.0, while C_{off} ranges from 0.3 to 0.7. Both parameters were also evaluated for the H I bubbles surrounding the Of stars HD 91572 and HD 91824, HD 94963, HD 112244, HD 152386, HD 155913, and HD 175758 and HD 175876 (Cappa & Benaglia 1998; Benaglia & Cappa 1999). C_{ax}-values are within the range 1.0 to 1.4, while C_{off} varies between 0.1 and 0.7. Similar values can also be obtained for H I bubbles related to WR stars (e.g., Niemela & Cappa de Nicolau 1991; Arnal 1992; Cappa et al. 1996a, 1996b; Arnal & Cappa 1996; Arnal & Roger 1997; Gervais & St-Louis 1999).

Most of the H I bubbles surrounding WR and Of stars are elliptical rather than spherical and most of the stars are eccentric with respect to the center of the bubbles. In addition, many stars are located closer to one of the highest density borders of the cavities. It is worth mentioning that the eccentric location is also seen in optical ring nebulae (e.g., Miller & Chu 1993; Marston et al. 1994).

Aspherical interstellar bubbles can be explained by relaxing some of the basic assumptions adopted in the classical

evolutionary models of interstellar bubbles (e.g., McCray 1983). An inhomogeneous ISM in the environs of the star and/or a star moving with a large spatial velocity with respect to its local ISM can easily favor the formation of distorted bubbles (e.g., Weaver et al. 1977; Dyson 1977; Icke 1988; Brighenti & D'Ercole 1995).

The spatial velocities of the stars can be derived from radial velocities and proper motions. The stellar radial velocities (see Table 1) are, in all cases, more negative than the systemic velocities of the associated H I bubbles. As pointed out by Conti, Leep, & Lorre (1977) and Gies (1987), Of stars show systematically negative velocities due to the atmospheric outflow, and consequently, their radial velocities are not reliable measures of their velocities in space. The radial velocities observed in direction to other O-type stars in Per OB1 are also more negative than what is expected from circular galactic rotation models (see Table 1). HD 12993 and HD 13268 are runaway stars (Cruz-González et al. 1974; McLachlan & Nandy 1985).

Proper motions for the O and Of stars related to the individual bubbles were looked for in the Tycho-2 Catalog (Hog et al. 2000). The components of the proper motions for these stars are below 2 σ except for HD 16691, for which the components are $\leq 3 \sigma$. In spite of the large uncertainties, the derived tangential velocities suggest that HD 16691 is moving away from the galactic plane. Taking into account the location of the star, this fact casts doubts on the H I structure–star association.

Taking these facts into account, an inhomogeneous ISM seems to be the most probable reason for the eccentric position of the star and the aspherical appearance of the probable H I bubbles in Per OB1.

Concerning the other O-type stars in the association, HD 12993, HD 14434 and Hilt 23 are close to the borders of the region surveyed with the Effelsberg radio telescope, and we were not able to examine their neighborhood with these data; while HDE 236894, HD 12323, HD 13268, HD13745, and HD 15642 are outside the surveyed region.

No H I bubble candidate was found to be related to HD 237019 within the velocity interval -50 to -15 km s^{-1}. Several reasons may be invoked in order to explain this fact. If present, the H I structure related to this star could be smaller than the HPBW of the Effelsberg radio telescope at 21 cm, i.e., $\simeq 5$ pc at 2.3 kpc. A high ambient gas density might be responsible for the small size of such bubble. On the other hand, confusion effects originated in the presence of fore- and background H I gas with velocities in the range -30 to -18 km s^{-1} might also mask an H I bubble related to this star.

6. SUMMARY

Based on H I 21 cm line observations, we have investigated the ISM in the vicinity of the O and Of stars belonging to the Per OB1 association, searching for the signatures of the interaction between the stellar wind and the surrounding gas.

The Effelsberg H I data (HPBW = 8.'4) allowed us to discover probable interstellar wind-blown bubbles associated with the massive Of stars HD 14442 [O5n(f)p] and HD 14947 [O5If+] and with the O stars HD 13022 [O9.5II-III((n))] and HD 13338 [O9.5V], while there are some doubts on the detection of an H I bubble related to HD 16691 [O5If+]. The dimensions of these interstellar bubbles are in the range 18–33 pc and their expansion

velocities are of about 10 km s^{-1}, implying dynamical ages of about $(1–2) \times 10^6$ yr. Infrared counterparts were also found for these bubbles. Our results indicate that the O and Of stars would be the main contributors to the shaping of the bubbles through stellar wind–ISM interaction. The H I bubbles discovered in Per OB1 share some characteristics with previously found H I interstellar bubbles related to WR and Of stars: (1) these new bubbles would be in the momentum-conserving case or in an intermediate stage between energy and momentum-conserving cases, (2) they are elliptical in shape, and (3) the O and Of stars responsible for their formation are projected at a eccentric position with respect to the center of the bubble.

We have also found a clear H I shell-like feature that seems to be related to the B1III stars HD 15233 and Hilt 311. Based on the present results, this feature cannot be explained as a wind-blown bubble. It must have been originated by a different mechanism.

The large-scale H I maps obtained with lower angular resolution data (HPBW = 36') enabled the identification of an H I shell that encircles the OB association Per OB1. The shell, which is 350×550 pc in size, could have been blown by Per OB1 as a whole. An IR counterpart of this shell was also found.

REFERENCES

Arnal, E. M. 1992, A&A, 254, 305
Arnal, E. M., & Cappa, C. E. 1996, MNRAS, 279, 788
Arnal, E. M., Cappa, C. E., Rizzo, J. R., & Cichowolski, S. 1999, AJ, 118, 1798
Arnal, E. M., & Roger, R. 1997, MNRAS, 285, 253
Becker, W., & Fenkart, R. 1971, A&AS, 4, 241
Benaglia, P., & Cappa. C. 1999, A&A, 346, 979
Brand, J., & Blitz, L. 1993, A&A, 275, 67
Brighenti, F., & D'Ercole, A. 1995, MNRAS, 273, 443
Bruhweiler, F. C., Gull, T. R., Kafatos, M., & Sofia, S. 1980, ApJ, 238, L27
Burton, W. B. 1988, In Galactic and Extragalactic Radio Astronomy, ed. G. L. Verschuur & K. I. Kellerman (2d ed.; Berlin: Springer), 295
Cappa, C. E., & Benaglia, P. 1998, AJ, 116, 1906
Cappa, C. E., Dubner, G. M., Rogers, C., & St-Louis, N. 1996a, AJ, 112, 1104
Cappa, C., Goss, W. M., Niemela, V., & Ostrov, P. 1999, AJ, 118, 948
Cappa, C. E., Niemela, V. S., Herbstmeier, U., & Koribalski, B. 1996b, A&A, 312, 283
Cappa de Nicolau, C. E., & Olano, C. A. 1990, Rev. Mex. Astron. Astrofis., 21, 273
Caswell, J. L., & Haynes, R. F. 1987, A&A, 171, 261
Chlebowski, T., & Garmany, C. D. 1991, ApJ, 368, 241
Chromey, F. R., Elmegreen, B. G., & Elmegreen, D. M. 1989, AJ, 98, 2303
Conti, P. S., Leep, E. M., & Lorre, J. J. 1977, ApJ, 214, 759
Cruz-González, C., Recillas-Cruz, E., Costero, R., Peimbert, M., & Torres-Peimbert, S. 1974, Rev. Mex. Astron. Astrofis., 1, 211
de Geus, E. J. 1988, Ph.D. thesis, Univ. Leiden
Dyson, J. E. 1977, A&A, 59, 161
Fürst, E., Reich, W., Reich, P., & Reif, K. 1990, A&AS, 85, 691
García-Segura, G., & Mac Low, M.-M. 1995, ApJ, 455, 145
Garmany, C. D., & Stencel, R. E. 1992, A&AS, 94, 211
Gervais, S., & St-Louis, N. 1999, AJ, 118, 2394
Gies, D. R. 1987, ApJS, 64, 545
Groenewegen, M. A. T., & Lamers, H. J. G. L. M. 1989, A&AS, 79, 359
Hartman, D., & Burton, W. B. 1997, Atlas of Galactic Neutral Hydrogen (Cambridge: Cambridge Univ. Press)
Heiles, C. 1979, ApJ, 229, 533
———. 1984, ApJS, 55, 585
Heyer, M. H., Brunt, C., Snell, R. L., Howe, J. E., Schloerb, F. P., & Carpenter, J. M. 1998, ApJS, 115, 241
Hog, E., Fabricius, C., Makarov, V. V., Urban, S., Corbin, T., Wycoff, G., Bastian, U., Schwekendiek, P., & Wicenec, A. 2000, A&A, 355, L27
Howarth, I. D., Siebert, K. W., Hussain, G. A. J., Prinja, R. K. 1997, MNRAS, 284, 265
Humphreys, R. 1978, ApJS, 38, 309
Icke, V. 1988, A&A, 202, 177
Janes, K., & Adler, D. 1982, ApJS, 49, 425
Kalberla, P. M. W., Mebold, U., & Reich, W. 1980, A&A, 82, 275
Kalberla, P. M. W., Mebold, U., & Reif, K. 1982, A&A, 106, 190

Kendall, T. R., Lennon, D. J., Brown, P. J. F., & Dufton, P. L. 1995, A&A, 298, 489
Kimeswenger, S., & Weinberger, R. 1989, A&A, 209, 51
Koo, B.-C., Heiles, C., & Reach, W. T. 1992, ApJ, 390, 108
Kuchar, T. A., & Bania, T. M. 1993, ApJ, 414, 664
Lamers, H. J. G. L. M., & Leitherer, C. 1993, ApJ, 412, 771
Leitherer, C. 1988, ApJ, 326, 356
Lockman, F. J. 1989, ApJS, 71, 469
Lozinskaya, T. A. 1982, Ap&SS, 87, 313
Mac Low, M.-M., & McCray, R. 1988, ApJ, 324, 776
Maeder, A., & Meynet, G. 1994, A&A, 287, 803
Marston, A. P. 1996, AJ, 112, 2828
Marston, A. P., Yocum, D. R., García-Segura, G., & Chu, Y.-H. 1994, ApJS, 95, 151
Mathys, G. 1989, A&AS, 81, 237
McCray, R. 1983, Highlights Astron., 5, 567
McCray, R., & Kafatos, M. 1987, ApJ, 317, 190
McLachlan, A., & Nandy, K. 1985, MNRAS, 215, 473
Miller, G., & Chu, Y.-H. 1993, ApJS, 85, 137
Münch, G. 1957, ApJ, 125, 42
Nicolet, B. 1978, A&AS, 34, 1
Niemela, V. S., & Cappa de Nicolau, C. E. 1991, AJ, 101, 572
Normandeau, M., Taylor, A. R., & Dewdney, P. E. 1996, Nature, 380, 687
Oey, M. S. 1996, ApJ, 467, 666
Parker, R. A. R., Gull, T. R., & Kirschner, R. P. 1979, An Emission Line Survey of the Milky Way, NASA SP No. 434
Phillips, A. P. & Gondhalekar, P. M. 1981, MNRAS, 196, 533
Prinja, R. K., Barlow, M. J., & Howarth, I. D. 1990, ApJ, 361, 607
Puls, J., et al. 1996, A&A, 305, 171
Reich, W., Reich, P., & Fürst, E. 1990, A&AS, 83, 539
Rizzo, J. R. 1994, Ph.D. thesis, Univ. Nac. La Plata
Rizzo, J. R., & Bajaja, E. 1994, A&A, 289, 922
Ruprecht, J. 1966, Trans. IAU, 12B, 350
Sancici, R. 1974, in IAU Symp. 60, Galactic Radio Astronomy, ed. F. J. Kerr & S. C. Simonson, III (Dordrecht: Reidel), 115
Schaerer, D., de Koter, A., Schmutz, W., &Maeder, A. 1996, A&A, 310, 837
Schmidt-Kaler, Th. 1982, in Landolt-Börnstein, Numerical Data and Functional Relationships in Science and Technology, ed. K. Schaifers & H. H. Voigt, Vol. VI/2b (New York: Springer), 1
Scuderi, S., Panagia, N., Stanghellini, C., Trigilio, C., & Umana, G. 1998, A&A, 332, 251
Simonson, S. C., & van Someren Greve, H. W. 1976, A&A, 49, 343
Treffers, R. R., & Chu, Y.-H. 1982, ApJ, 254, 569
Underhill, A. B., & Gilroy, K. K. 1990, ApJ, 364, 626
Vacca, W. D., Garmany, C. D., & Schull, J. M. 1996, ApJ, 460, 914
Walborn, N. 1972, AJ, 77, 312
———. 1973, AJ, 78, 1067
Weaver, R., McCray, R., Castor, J., Shapiro, P., & Moore, R. 1977, ApJ, 218, 377
Wrigge, M. 1999, A&A, 343, 599